Supporting Information

A Spectroscopic Investigation of the Primary Reaction Intermediates in the Oxidation of Levitated Droplets of Energetic Ionic Liquids

Stephen J. Brotton,[1] Michael Lucas,[1] Steven D. Chambreau,[2] Ghanshyam L. Vaghjiani,[3] Jiang Yu,[4] Scott L. Anderson,[4] and Ralf I. Kaiser[1]

[1] Department of Chemistry, University of Hawaii at Manoa, Honolulu, HI 96822

[2] ERC Inc., Edwards Air Force Base, CA 93524.

[3] In-Space Propulsion Branch, Rocket Propulsion Division, Aerospace Systems Directorate, Air Force Research Laboratory, AFRL/RQRS, Edwards Air Force Base, CA 93524.

[4] University of Utah, Department of Chemistry, Salt Lake City, UT 84112.

Experimental Methods

A single droplet of the ionic liquid was levitated in an ultrasonic levitator enclosed within a pressure-compatible process chamber. The apparatus has been discussed in detail elsewhere.[1-2] The chamber was evacuated and then filled to 880 Torr with argon (Airgas, 99.9999%) or a gas mixture of 1.3% nitrogen dioxide (Aldrich, $\geq$ 99.5%) and 98.7% argon. The 1-methyl-4-amino-1,2,4-triazolium dicyanamide ([MAT][DCA]) was synthesized as discussed in reference 3. The [MAT][DCA]-capped, hydrogen-terminated boron nanoparticles were produced by high-energy ball-milling boron powder in a hydrogen atmosphere, resulting in hydrogen-terminated nanoparticles, and then capping with [MAT][DCA] to generate air-stable, unoxidized particles, as described in reference 4. A piezoelectric transducer oscillating at 58 kHz generates ultrasonic sound waves that reflect multiple times between the transducer and a concave-shaped reflector to create the standing wave that levitates the droplet. The [MAT][DCA] or [MAT][DCA] with boron nanoparticles was injected into the center of the levitator using a syringe and needle to form a droplet with a diameter of typically 1 mm. The chemical modifications of the levitated droplets were monitored *in situ* by Raman[1-2, 5] and UV-visible (StellarNet Inc., Silver-Nova) spectrometers. The Raman transitions are excited by the 532 nm line of a diode-pumped, Q-switched Nd:YAG laser. The Raman-shifted photons, which were backscattered from the droplet, are focused by a lens into a HoloSpec *f* /1.8 holographic imaging spectrograph equipped with a PI-Max 2 ICCD camera from Princeton Instruments. In the UV-visible spectrometer, the output from a high-brightness UV-visible source is transmitted via a fiber-optic feedthrough on a 35 CF flange to a reflectance probe located inside of the vacuum chamber. The backscattered light is collected by a read fiber, exits the chamber via a different connector on the same 35 CF fiber-optic feedthrough, and finally enters a UV-visible spectrometer that covers the 190 nm to 1100 nm spectral range. The Fourier-transform infrared (FTIR) spectra were taken before and after the reaction using an attenuated total reflection (ATR) accessory with a Thermo Scientific Nicolet 6700 FTIR spectrometer.[1]

Computational Methods

A variant of the quantum-mechanical continuum solvation model SMD,[6] known as the generic ionic liquid (SMD-GIL) model,[7] was employed to calculate the vibrational frequencies of the reactants and products in the condensed phase of the ionic liquid. The SMD-GIL calculations were performed using Gaussian 09[8] with an M06/6-31+G(d,p) basis set. In detail, the SMD-GIL solvent descriptor input parameters used to simulate [MAT][DCA] as the solvent are: $e = 11.50$, $n = 1.4300$, $\gamma = 61.24$, $\Sigma\alpha_2^H = 0.229$, $\Sigma\beta_2^H = 0.265$, $\varphi = 0.2308$, and $\psi = 0.0000$.[7] After calculating the frequencies, a scaling factor is needed for agreement between experiment and theory. For the M06 level of theory used here, all the vibrational frequencies presented have therefore been scaled by the factor of 0.989.

To interpret the UV-visible spectra in the 200 - 1100 nm wavelength range, we investigated the electronic transitions of each relevant species. Time-dependent density functional theory (TD-DFT) at the M06/6-31 + G(d,p) level was therefore applied to [MAT][DCA], NO_2, and [MAT][DCA] bonded with NO_2 as shown in Figure 1. The calculations were performed using Gaussian09 for the first 50 electronic transitions of each species including singlets and triplets states. The electronic transitions were assigned, for example to $\pi \rightarrow \pi^*$ or $\pi^* \rightarrow \pi^*$, by visual inspection of the molecular orbitals involved in each transition.

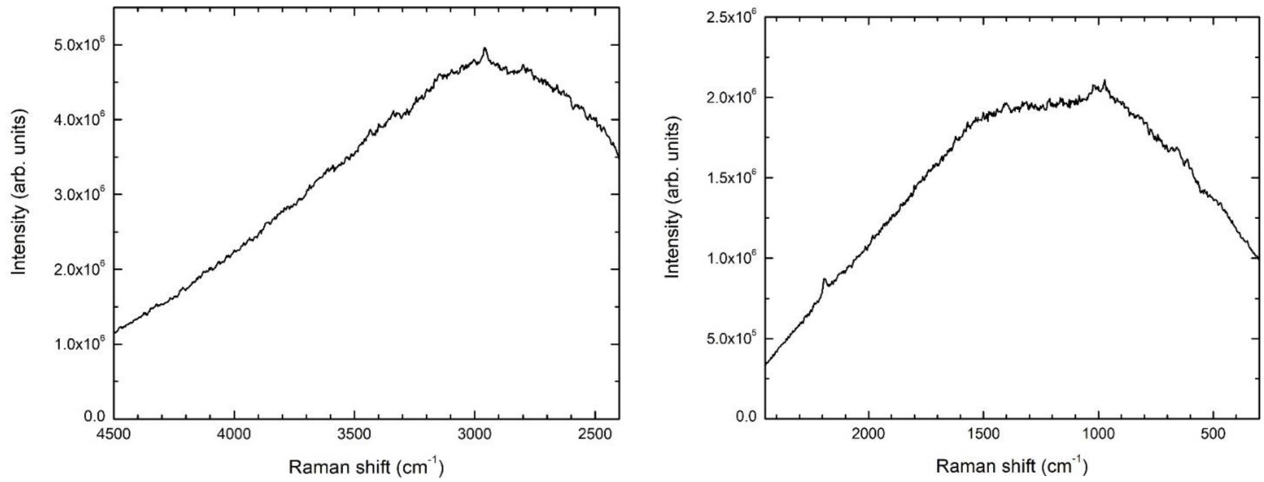

Figure S1. Raman spectra of [MAT][DCA] with hydrogen-capped, boron nanoparticles levitated in argon.

Table S1. Assignments for the observed peaks in the infrared spectra of [MAT][DCA] and [MAT][DCA] doped with hydrogen-capped boron nanoparticles by comparison with GIL theoretical values for [MAT][DCA], the measured values in [a] Ref. [9], [b] Ref. [10], [c] Ref. [11] for the $[DCA]^-$ anion, and [d] Ref. [12] for the B-H bond

number	vibrational mode	theoretical and measured reference wavenumbers (cm^{-1})	measured wavenumbers [MAT][DCA] (cm^{-1})	measured wavenumbers boron-doped [MAT][DCA] (cm^{-1})
ν_1	$[DCA]^-$ wag	31		
ν_2	$[DCA]^-$ rock	45		
ν_3	$[DCA]^-$ rock	54		
ν_4	$[DCA]^-$ rock	75		
ν_5	$[DCA]^-$ rock	94		
ν_6	$N(CN)_2$ bend $[DCA]^-$	140		
ν_7	CH_3 rock	173		
ν_8	CH_3 rotation	196		
ν_9	out-of-plane symmetric NH_2, CH_3 wag	231		
ν_{10}	out-of-plane symmetric NH_2, CH_3 wag 2	290		
ν_{11}	NH_2 rock	302		
ν_{12}	NH_2 rotation	335		
ν_{13}	antisymmetric NH_2, CH_3 in-plane wag	450		
ν_{14}	in-plane antisymmetric N-C≡N bend of $[DCA]^-$	514		
ν_2*	in-plane antisymmetric N-C≡N bend of $[DCA]^-$	517a)	511	512
ν_3*	out-of-plane antisymmetric N-C≡N bend of $[DCA]^-$	530a)	524	524
ν_4*	out-of-plane symmetric N-C≡N bend of $[DCA]^-$	543a)	540	540
ν_{15}	out-of-plane symmetric N-C≡N bend of $[DCA]^-$	541		
ν_{16}	out-of-plane antisymmetric N-C≡N bend of $[DCA]^-$	554		
ν_{17}	symmetric N-NH_2 and N-CH_3 stretch	613	601	601
ν_{18}	N(4) umbrella	620	613	613
ν_{19}	in-plane symmetric N-C-N bend in $[DCA]^-$	651		
ν_{20} ν_5*	$H_3CN(1)$-N(2)CH torsion in-plane C-N-C bend of $[DCA]^-$	659 666b)	657	657
ν_{21}	antisymmetric ring mode with N-CH_3 and N-NH_2 stretch	747	737	737
ν_{22} ν_{23}	C(3)H, C(5)H antisymmetric out-of-plane wag C(3)H, C(5)H symmetric out-of-plane wag	871 892	880	878
ν_6*	C-N-C symmetric stretch of $[DCA]^-$	904b)	905	905
ν_{24}	C-N-C symmetric stretch in $[DCA]^-$	936		
ν_{25}	NH_2 rock	958		
ν_{26}	N(1)-N(2) stretch, C(3)H in-plane wag	993	978	978

ν_{27}	ring C-N-C symmetric stretch, C(5) wag and CH_3 rock	1059	1071	1071
ν_{28}	N-C-N ring bend, CH_3 rock	1085	1091	1091
ν_{29}	CH_3 rock	1120		
ν_{30}	C(5)H wag, N(1)-CH_3 stretch	1168	1171	1170
ν_{31}	C(3)H, C(5)H antisymmetric in-plane wag	1197	1212	1213
ν_{32}	ring NN stretch	1287		
ν_7*	C-N-C antisymmetric stretch of $[DCA]^-$	1309[b)]	1310	1310
ν_{33}	ring C-N-C antisymmetric stretch, NH_2 rock	1354		
ν_{34}	ring C-N-C antisymmetric stretch, NH_2 rock 2	1382		
ν_{35}	CH_3 umbrella	1396		
ν_{36}	C-N-C antisymmetric stretch in $[DCA]^-$	1403		
ν_{37}	CH_2 wag	1405	1407	1407
ν_{38}	CH_2 wag 2	1418	1439	1439
ν_{39}	N(2)-C(3) and N(4)-C(5) symmetric stretch	1455	1455	1456
ν_{40}	N(2)-C(3) and N(4)-C(5) antisymmetric stretch	1566	1535	1535
ν_{41}	N(1)-C(5) stretch, N-NH_2 and N-CH_3 antisymmetric stretch	1588	1571	1570
ν_{42}	NH_2 scissor	1638	1630	1630
ν_8*	C≡N antisymmetric stretch of $[DCA]^-$	2133[b)]	2126	2126
ν_9*	C≡N symmetric stretch of $[DCA]^-$	2192[b)]	2197	2197
ν_6*+ν_7*	$[DCA]^-$ combination mode	2227[c)]	2237	2237
ν_{43}	$[DCA]^-$ antisymmetric stretch	2232		
ν_{44}	$[DCA]^-$ symmetric stretch	2275		
ν(B-H)	B-H stretch	2565-2480[d)]	-	2494
ν_{45}	CH_3 symmetric stretch	3038	2971	2971
ν_{46}	CH_3 antisymmetric stretch	3148	3022	3021
ν_{47}	CH_3 antisymmetric stretch 2	3162	3080	3079
ν_{48}	C(5)H stretch	3234	3142	3141
ν_{49}	C(3)H stretch	3242	3227	3218
ν_{50}	symmetric NH stretch	3317	3294	3291
ν_{51}	antisymmetric NH stretch	3527	3507	3505

Table S2. Assignments for the observed peaks in the Raman spectrum of [MAT][DCA] by comparison with GIL theoretical values for [MAT][DCA], and the measured values in [a] Ref. [9], [b] Ref. [10], [c] Ref. [11] for the $[DCA]^-$ anion.

number	vibrational mode	theoretical and measured reference wavenumbers (cm^{-1})	measured wavenumbers [MAT][DCA] (cm^{-1})
ν_1	$[DCA]^-$ wag	31	
ν_2	$[DCA]^-$ rock	45	
ν_3	$[DCA]^-$ rock	54	
ν_4	$[DCA]^-$ rock	75	
ν_5	$[DCA]^-$ rock	94	
ν_6	$N(CN)_2$ bend $[DCA]^-$	140	
ν_7	CH_3 rock	173	
ν_8	CH_3 rotation	196	
ν_9	out-of-plane symmetric NH_2, CH_3 wag	231	
ν_{10}	out-of-plane symmetric NH_2, CH_3 wag 2	290	
ν_{11}	NH_2 rock	302	
ν_{12}	NH_2 rotation	335	
ν_{13}	antisymmetric NH_2, CH_3 in-plane wag	450	446
ν_{14}	in-plane antisymmetric N-C≡N bend of $[DCA]^-$	514	
ν_3*	out-of-plane symmetric N-C≡N bend of $[DCA]^-$	530[a)]	532
ν_{15}	out-of-plane symmetric N-C≡N bend of $[DCA]^-$	541	
ν_{16}	out-of-plane antisymmetric N-C≡N bend of $[DCA]^-$	554	
ν_{17}	symmetric $N-NH_2$ and $N-CH_3$ stretch	613	606
ν_{18}	N(4) umbrella	620	
ν_{19}	in-plane symmetric N-C-N bend in $[DCA]^-$	651	
ν_{20} ν_5*	$H_3CN(1)-N(2)CH$ torsion in-plane C-N-C bend of $[DCA]^-$	659 666[b)]	655
ν_{21}	antisymmetric ring mode with $N-CH_3$ and $N-NH_2$ stretch	747	729
ν_{22}	C(3)H, C(5)H antisymmetric out-of-plane wag	871	863
ν_{23} ν_6*	C(3)H, C(5)H symmetric out-of-plane wag C-N-C symmetric stretch of $[DCA]^-$	892 904[b)]	897
ν_{24}	C-N-C symmetric stretch in $[DCA]^-$	936	
ν_{25}	NH_2 rock	958	971
ν_{26}	N(1)-N(2) stretch, C(3)H in-plane wag	993	1038
ν_{27}	ring C-N-C symmetric stretch, C(5) wag and CH_3	1059	1059

	rock		
ν_{28}	N-C-N ring bend, CH_3 rock	1085	1077
ν_{29}	CH_3 rock	1120	
ν_{30}	C(5)H wag, N(1)-CH_3 stretch	1168	1163
ν_{31}	C(3)H, C(5)H antisymmetric in-plane wag	1197	1206
ν_{32}	ring NN stretch	1287	
ν_7*	C-N-C antisymmetric stretch of $[DCA]^-$	1309[b)]	1315
ν_{33}	ring C-N-C antisymmetric stretch, NH_2 rock	1354	
ν_{34}	ring C-N-C antisymmetric stretch, NH_2 rock 2	1382	
ν_{35}	CH_3 umbrella	1396	
ν_{36}	C-N-C antisymmetric stretch in $[DCA]^-$	1403	
ν_{37}	CH_3 umbrella	1405	1402
ν_{38}	CH_2 wag 2	1418	
ν_{39}	N(2)-C(3) and N(4)-C(5) symmetric stretch	1455	1448
ν_{40}	N(2)-C(3) and N(4)-C(5) antisymmetric stretch	1566	1530
ν_{41}	N(1)-C(5) stretch, N-NH_2 and N-CH_3 antisymmetric stretch	1588	1566
ν_{42}	NH_2 scissor	1638	1624
ν_8*	C≡N antisymmetric stretch of $[DCA]^-$	2133[b)]	2132
ν_9*	C≡N symmetric stretch of $[DCA]^-$	2192[b)]	2191
ν_6*+ ν_7*	$[DCA]^-$ combination mode	2227[c)]	2236
ν_{43}	$[DCA]^-$ antisymmetric stretch	2232	
ν_{44}	$[DCA]^-$ symmetric stretch	2275	
$2\nu_{37}$	antisymmetric mixed mode	2804	2803
ν_{45}	CH_3 symmetric stretch	3038	2954
ν_{46}	CH_3 antisymmetric stretch	3148	3029
ν_{47}	CH_3 antisymmetric stretch 2	3162	3109
ν_{48} ν_{49}	C(5)H stretch C(3)H stretch	3234 3242	3160
ν_{50}	symmetric NH stretch	3317	3319

Table S3. Theoretical wavenumbers and vibrational mode assignments for [MAT][DCA] bonded with nitrogen dioxide (Figure 1) calculated using the SMD-GIL model at the M06/6-31+G(d,p) level of theory.

number	vibrational mode	theoretical wavenumbers (cm^{-1})
ν_1	NO_2 rock	11
ν_2	anion rock 1	32
ν_3	anion rock 2	44
ν_4	N=C=N wag	65
ν_5	Cation rock	69
ν_6	CH_3 to NO_2 stretch	94
ν_7	C-N-CN bend of anion	98
ν_8	O_2NN-CNCN torsion	138
ν_9	CH_3 rotation	159
ν_{10}	CH_3 rotation and C-N-CN bend	177
ν_{11}	CH_3 rotation and N(4)C(3)-N(2)CH_3 torsion	215
ν_{12}	C=N-NO_2 in-plane bend	224
ν_{13}	NH_2 wag	291
ν_{14}	NH_2 wag and N-N-CH_3 in plane bend	307
ν_{15}	C=N=C=N out-of-plane torsion + NH_2 rotation	332
ν_{16}	O_2N-NC torsion in anion	354
ν_{17}	O_2NN=C=N in-plane bend + N-C≡N bend	432
ν_{18}	antisymmetric NH_2 and CH_3 in plane wag	456
ν_{19}	N-C≡N out-of-plane bend	570
ν_{20}	NO_2 rock + N=C=N in-plane bend + C(3)H bend	608
ν_{21}	N-NH_2 + N-CH_3 symmetric in-plane bend	611
ν_{22}	C(3) + C(5) out-of-plane symmetric bend	618
ν_{23}	N-C≡N in-plane bend	653
ν_{24}	N(4) + C(5) out-of-plane bend	661
ν_{25}	N-N=C bend + C(5)H in-plane wag	745
ν_{26}	N-NO_2 umbrella	779
ν_{27}	N=C=N-NO_2 bend + N-NO_2 umbrella	784
ν_{28}	C(3)H + C(5)H out-of-plane antisymmetric wag	876
ν_{29}	C(3)H + C(5)H out-of-plane symmetric wag	896
ν_{30}	N-NO_2 symmetric stretch	946
ν_{31}	N-NO_2 symmetric stretch + NH_2 wag	982
ν_{32}	ring NN stretch + NH_2 wag	996
ν_{33}	N-CN stretch	1029
ν_{34}	C(3)H + C(5)H in-plane wag	1054
ν_{35}	CH_3 in-plane rocking	1085

ν_{36}	CH_3 out-of-plane rocking	1125
ν_{37}	C(3)H in-plane wag	1161
ν_{38}	C(5)H in-plane wag	1201
ν_{39}	C=N-NO_2 stretch	1271
ν_{40}	ring NN stretch + CH_2 wag + C(3)H + C(5)H in-plane symmetric wag	1288
ν_{41}	N=C=N-NO_2 symmetric stretch + NH_2 rock	1351
ν_{42}	ring CNC antisymmetric stretch	1355
ν_{43}	NH_2 rock	1370
ν_{44}	CH_3 umbrella	1398
ν_{45}	ring breathing + CH_3 antisymmetric wag 1	1429
ν_{46}	ring breathing + CH_3 antisymmetric wag 2	1405
ν_{47}	ring breathing + CH_3 antisymmetric wag 3	1420
ν_{48}	ring CNNC antisymmetric stretch + C(3)H in-plane wag	1456
ν_{49}	O=N=O antisymmetric stretch	1568
ν_{50}	ring CNNC symmetric stretch + C(3)H in-plane wag	1576
ν_{51}	NH_2 bend	1585
ν_{52}	O_2N-NC=NCN stretch	1632
ν_{53}	N-C≡N antisymmetric stretch	2256
ν_{54}	CH_3 symmetric stretch	3032
ν_{55}	C(5)H stretch	3145
ν_{56}	CH_2 antisymmetric stretch	3147
ν_{57}	CH_3 antisymmetric stretch	3152
ν_{58}	C(3) + NH_2 antisymmetric stretch	3254
ν_{59}	C(3) + NH_2 symmetric stretch	3372
ν_{60}	NH_2 antisymmetric stretch	3532

Table S4. Cartesian coordinates of the atoms in [MAT][DCA] and [MAT][DCA] reacted with nitrogen dioxide calculated at the M06/6-31+G(d,p) level of theory.

structure	coordinates (Å)			
[MAT][DCA] 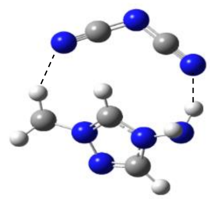	C	0.944	0.020	-0.821
	C	2.064	-0.583	0.940
	N	1.357	1.077	-0.152
	H	0.364	0.012	-1.736
	H	2.530	-1.234	1.667
	C	1.162	2.484	-0.467
	H	0.605	2.555	-1.402
	H	0.593	2.950	0.340
	H	2.142	2.955	-0.570
	N	2.058	0.721	0.958
	N	1.388	-1.056	-0.146
	N	1.215	-2.407	-0.436
	H	0.209	-2.611	-0.360
	H	1.537	-2.574	-1.388
	N	-2.959	-0.119	0.288
	C	-2.254	-1.196	0.134
	C	-2.444	1.069	0.144
	N	-1.688	-2.222	0.009
	N	-2.057	2.175	0.031
[MAT][DCA] + NO_2 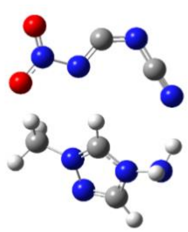	C	1.277	-0.354	0.345
	C	3.410	-0.356	-0.085
	N	1.605	-1.404	-0.380
	H	0.273	-0.090	0.671
	H	4.440	-0.028	-0.087
	C	0.731	-2.448	-0.893
	H	-0.268	-2.298	-0.476
	H	0.706	-2.384	-1.983
	H	1.127	-3.417	-0.581
	N	2.937	-1.427	-0.660
	N	2.416	0.333	0.547
	N	2.606	1.535	1.224
	H	1.982	2.230	0.798
	H	2.356	1.399	2.202
	N	-1.914	2.295	-0.741
	C	-0.636	2.554	-0.576
	C	-2.430	1.172	-0.397
	N	0.495	2.840	-0.454
	N	-1.883	0.098	0.116
	N	-2.749	-0.932	0.407
	O	-3.958	-0.833	0.228
	O	-2.208	-1.941	0.857

References

1. Brotton, S. J.; Kaiser, R. I., Novel High-Temperature and Pressure-Compatible Ultrasonic Levitator Apparatus Coupled to Raman and Fourier Transform Infrared Spectrometers. *Rev. Sci. Instrum.* **2013,** *84*, 055114.
2. Brotton, S. J.; Kaiser, R. I., In Situ Raman Spectroscopic Study of Gypsum ($CaSO_4$ • $2H_2O$) and Epsomite ($MgSO_4$ • $7H_2O$) Dehydration Utilizing an Ultrasonic Levitator. *J. Phys. Chem. Lett.* **2013,** *4*, 669-673.
3. Hawkins, T. W.; Schneider, S.; Drake, G. W.; Vaghjiani, G.; Chambreau, S. Hypergolic Fuels Containing Fuel and Oxidizer for Liquid Rockets or Propellants. U.S. Patent 8034202B1, 2011.
4. Perez, J. P. L.; Yu, J.; Sheppard, A. J.; Chambreau, S. D.; Vaghjiani, G. L.; Anderson, S. L., Binding of Alkenes and Ionic Liquids to B-H-Functionalized Boron Nanoparticles: Creation of Particles with Controlled Dispersibility and Minimal Surface Oxidation. *ACS Appl. Mater. Interfaces* **2015,** *7*, 9991-10003.
5. Bennett, C. J.; Brotton, S. J.; Jones, B. M.; Misra, A. K.; Sharma, S. K.; Kaiser, R. I., High-Sensitivity Raman Spectrometer To Study Pristine and Irradiated Interstellar Ice Analogs. *Anal. Chem.* **2013,** *85*, 5659-5665.
6. Marenich, A. V.; Cramer, C. J.; Truhlar, D. G., Universal Solvation Model Based on Solute Electron Density and on a Continuum Model of the Solvent Defined by the Bulk Dielectric Constant and Atomic Surface Tensions. *Journal of Physical Chemistry B* **2009,** *113*, 6378-6396.
7. Bernales, V. S.; Marenich, A. V.; Contreras, R.; Cramer, C. J.; Truhlar, D. G., Quantum Mechanical Continuum Solvation Models for Ionic Liquids. *J. Phys. Chem. B* **2012,** *116*, 9122-9129.
8. Frisch, M. J. T., G. W.; Schlegel, H. B.; Scuseria, G. E.; Robb, M. A.; Cheeseman, J. R.; Scalmani, G.; Barone, V.; Mennucci, B.; Petersson, G. A., et al., Gaussian 09, Revision A.02. *Gaussian, Inc.: Wallingford, CT, 2009*.
9. Reckeweg, O.; DiSalvo, F. J.; Schulz, A.; Blaschkowski, B.; Jagiella, S.; Schleid, T., Synthesis, Crystal Structure, and Vibrational Spectra of the Anhydrous Lithium Dicyanamide Li $N(CN)_2$. *Z. Anorg.Allg. Chem.* **2014,** *640*, 851-855.
10. Paschoal, V. H.; Faria, L. F. O.; Ribeiro, M. C. C., Vibrational Spectroscopy of Ionic Liquids. *Chem. Rev.* **2017,** *117*, 7053-7112.
11. Kiefer, J.; Noack, K.; Penna, T. C.; Ribeiro, M. C. C.; Weber, H.; Kirchner, B., Vibrational Signatures of Anionic Cyano Groups in Imidazolium Ionic Liquids. *Vib. Spectros.* **2017,** *91*, 141-146.
12. Socrates, G., *Infrared and Raman Characteristic Group Frequencies : Tables and Charts*. 3rd ed.; Wiley: Chichester ; New York, 2001.